

# Globally-Attractive Logarithmic Geometric Control of a Quadrotor for Aggressive Trajectory Tracking

Jacob Johnson<sup>1</sup>, Randal Beard<sup>2</sup>

**Abstract**—We present a new quadrotor geometric control scheme that is capable of tracking highly aggressive trajectories. Unlike previous works, our geometric controller uses the logarithmic map of  $SO(3)$  to express rotational error in the Lie algebra, allowing us to treat the manifold in a more effective and natural manner, and can be shown to be globally attractive. We show the performance of our control scheme against highly aggressive trajectories in simulation experiments. Additionally, we present an adaptation of this controller that allows us to interface effectively with the angular rate controllers on an onboard flight control unit and show the ability of this adapted control scheme to track aggressive trajectories on a quadrotor hardware platform.

## I. INTRODUCTION

A large number of quadrotor control methods have been presented in the literature. These methods can be sorted into three general categories: those that are linear, those that are nonlinear and non-geometric, and those that are geometric. Linear control methods neglect or approximate the nonlinear dynamics of the quadrotor by linearizing about an equilibrium point and treating the resulting dynamics as if they were the true dynamics of the system. These methods perform well as long as the state of the system remains near the equilibrium, but fail when the state leaves the resulting region of attraction.

Nonlinear non-geometric control methods (e.g. [1]) compensate for certain nonlinearities in the dynamics of the quadrotor and are attractive for large regions of attraction [2]. However, they neglect the fact that the rotation states of the quadrotor belong to a Lie group, the special orthogonal group  $SO(3)$ . These control methods usually approximate the rotation states as a vector of Euler angles, resulting in poor performance when the rotation of the quadrotor approaches the associated singularities, or as a unit quaternion, resulting in possible unwinding phenomena.

Geometric control methods correctly model the rotation states on  $SO(3)$  and are derived using methods from differential geometry. They can stabilize the quadrotor dynamics for almost any initial rotation. The seminal work for quadrotor geometric control is [3]. Because of its ability to track aggressive trajectories, this controller has been used in the literature for over a decade (e.g. [4], [5]).

<sup>1</sup>Graduate research assistant, Electrical and Computer Engineering, Brigham Young University, [jjohns99@byu.edu](mailto:jjohns99@byu.edu)

<sup>2</sup>Professor of Electrical and Computer Engineering, Brigham Young University, [beard@byu.edu](mailto:beard@byu.edu)

\*This work has been funded by the Center for Unmanned Aircraft Systems (C-UAS), a National Science Foundation Industry/University Cooperative Research Center (IUCRC) under NSF award No. IIP-1650547, along with significant contributions from C-UAS industry members.

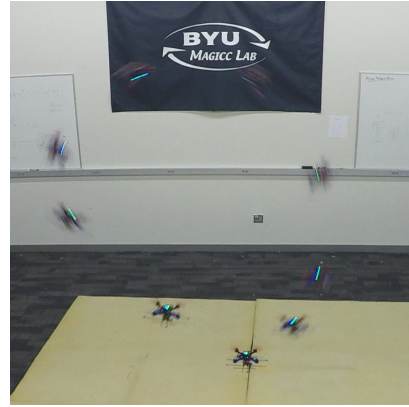


Fig. 1. Time lapse image of our proposed geometric control scheme tracking a flipping loop trajectory.

While the controller derived in [3] has been shown to perform well for aggressive trajectory tracking, it does not do well at recovering the quadrotor from configurations where the body rotation is close to 180 degrees from the desired rotation. This is because the magnitude of the rotational error vector in [3] goes to zero as the error rotation approaches 180 degrees. Lee acknowledged this in [6] and developed a new attitude error function that does not have this issue. However, the error function in [6] seems to lack motivation from the physics or dynamics of the system.

Because the exponential map from the Lie algebra to the Lie group corresponds to geodesics, or shortest paths, its inverse, the logarithmic map, is the most intuitive and effective way to represent error on Lie groups. Expressing error in the Lie algebra is advantageous because it is a vector space, meaning that vector operations can be performed on its elements, making them much easier to work with than elements of the Lie group itself.

The estimation literature has widely adopted the use of the logarithmic map to represent error in poses and rotations (see e.g. [7], [8], [9]). However, it seems that it has not been widely used in the quadrotor control literature. The only examples that the authors were able to find were [10], where it was applied to finite-time sliding mode control, and [11], where it was used for attitude regulation.

In this paper, we present a new geometric quadrotor control scheme that uses the logarithmic map to express the quadrotor rotation error in the tangent space of  $SO(3)$ . Our geometric controller is an adaptation of the one presented in [12], however, we prove that ours is globally attractive, even when the initial rotation error is exactly 180 degrees. We

incorporate this controller in a full trajectory tracking scheme and show its ability to track highly aggressive trajectories in simulation. Additionally, we develop an adaptation that allows it to interface with the angular rate controllers that run at very high rates on an onboard embedded flight control unit (FCU), and present highly aggressive trajectory tracking results of this controller on a quadrotor hardware platform.

## II. PRELIMINARIES

We use the vector notation  $\mathbf{t}_{a/b}^c \in \mathbb{R}^3$  to denote a value  $\mathbf{t}$  (e.g. position, velocity) of coordinate frame  $a$  with respect to frame  $b$  expressed in frame  $c$ . Thus  $\mathbf{t}_{a/b}^c = -\mathbf{t}_{b/a}^c$  and  $\mathbf{t}_{a/b}^a = \mathbf{R}_c^a \mathbf{t}_{a/b}^c$ , where  $\mathbf{R}_c^a$  is a rotation matrix that re-expresses vectors from frame  $c$  to frame  $a$ . The set of all 3D rotation matrices is isomorphic to the special orthogonal group, which can therefore be expressed as

$$\text{SO}(3) = \{\mathbf{R} \in \mathbb{R}^{3 \times 3} \mid \mathbf{R}^\top \mathbf{R} = \mathbf{I}, \det(\mathbf{R}) = 1\}, \quad (1)$$

equipped with the group action of matrix multiplication. This set satisfies the group axioms and forms a smooth manifold, making  $\text{SO}(3)$  a Lie group. The Lie algebra of  $\text{SO}(3)$  (denoted  $\mathfrak{so}(3)$ ) is the set of  $3 \times 3$  skew-symmetric matrices and is isomorphic to  $\mathbb{R}^3$  under the hat map

$$\phi^\wedge = \begin{bmatrix} 0 & -\phi_3 & \phi_2 \\ \phi_3 & 0 & -\phi_1 \\ -\phi_2 & \phi_1 & 0 \end{bmatrix} \quad (2)$$

for  $\phi \in \mathbb{R}^3$ . Skew-symmetric matrices can be mapped back to  $\mathbb{R}^3$  using the vee map  $(\phi^\wedge)^\vee = \phi$ . For  $\mathbf{R} \in \text{SO}(3)$ ,

$$(\mathbf{R}\phi)^\wedge = \mathbf{R}\phi^\wedge \mathbf{R}^\top, \quad (3)$$

and for  $\mathbf{a}, \mathbf{b} \in \mathbb{R}^3$ ,  $\mathbf{a}^\wedge \mathbf{b} = -\mathbf{b}^\wedge \mathbf{a}$ .

The exponential map

$$\text{Exp}(\phi) = \mathbf{I} + \sin(\phi) \mathbf{u}^\wedge + (1 - \cos(\phi)) \mathbf{u}^\wedge \mathbf{u}^\wedge, \quad (4)$$

where  $\phi = \phi \mathbf{u}$  and  $\mathbf{u}$  is a unit vector, can be used to map from  $\mathbb{R}^3$  to  $\text{SO}(3)$ . Its inverse is the logarithmic map

$$\phi \mathbf{u} = \text{Log}(\mathbf{R}) = \frac{\phi}{2\sin(\phi)} (\mathbf{R} - \mathbf{R}^\top)^\vee \quad (5)$$

$$\phi = \cos^{-1} \left( \frac{\text{tr}(\mathbf{R}) - 1}{2} \right). \quad (6)$$

Additionally, we will make use of the left Jacobian of  $\text{SO}(3)$

$$\begin{aligned} J_l(\phi) &= \mathbf{I} + \frac{1 - \cos(\phi)}{\phi} \mathbf{u}^\wedge + \frac{\phi - \sin(\phi)}{\phi} \mathbf{u}^\wedge \mathbf{u}^\wedge \\ &= \int_0^1 \text{Exp}(\phi)^\alpha d\alpha \end{aligned} \quad (7)$$

and its inverse

$$J_l^{-1}(\phi) = \mathbf{I} - \frac{\phi}{2} \mathbf{u}^\wedge + \left( 1 - \frac{\phi + \phi \cos(\phi)}{2\sin(\phi)} \right) \mathbf{u}^\wedge \mathbf{u}^\wedge. \quad (8)$$

The closed-form expressions of the logarithmic map, the left Jacobian, and its inverse are not globally defined because of their singularities at  $\phi = m\pi$ , where  $m \in \mathbb{Z}$ . However, we determine what their values at these singularities are in the Appendix.

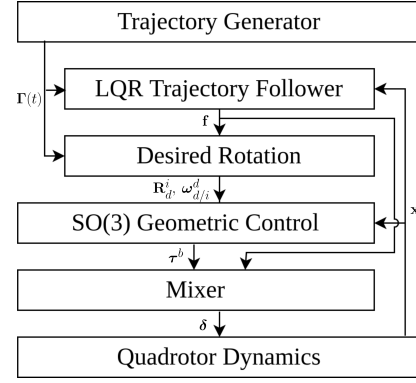


Fig. 2. The architecture of the proposed control scheme.

## III. QUADROTOR DYNAMICS

The state of the quadrotor is given by the tuple  $\mathbf{x} = (\mathbf{p}_{b/i}^i, \mathbf{v}_{b/i}^i, \mathbf{R}_b^i, \boldsymbol{\omega}_{b/i}^i)$ , where  $\mathbf{p}_{b/i}^i$  and  $\mathbf{v}_{b/i}^i \in \mathbb{R}^3$  are the position and velocity of the body frame (the coordinate system whose origin lies at the center of mass of the vehicle, with the  $i$  and  $j$  axes pointing out the front and right sides of the vehicle and the  $k$  axis pointing out its underside) expressed in some north-east-down inertial frame,  $\mathbf{R}_b^i \in \text{SO}(3)$  is the rotation from the body frame to the inertial frame, and  $\boldsymbol{\omega}_{b/i}^i$  is the angular velocity of the body frame expressed in the body frame.

We model the dynamics of the quadrotor using the equations [13]

$$\dot{\mathbf{p}}_{b/i}^i = \mathbf{v}_{b/i}^i, \quad (9a)$$

$$\dot{\mathbf{v}}_{b/i}^i = g\mathbf{e}_3 - \frac{T}{m} \mathbf{R}_b^i \mathbf{e}_3, \quad (9b)$$

$$\dot{\mathbf{R}}_b^i = \mathbf{R}_b^i \boldsymbol{\omega}_{b/i}^i{}^\wedge, \quad (9c)$$

$$\mathbf{J} \dot{\boldsymbol{\omega}}_{b/i}^i = -\boldsymbol{\omega}_{b/i}^i{}^\wedge \mathbf{J} \boldsymbol{\omega}_{b/i}^i + \boldsymbol{\tau}^b, \quad (9d)$$

where  $g$  is the gravitational constant,  $m$  is the mass of the vehicle,  $\mathbf{J} \in \mathbb{R}^{3 \times 3}$  is the inertia matrix,  $T$  is the total force produced by the rotors,  $\boldsymbol{\tau}^b \in \mathbb{R}^3$  is the total moment vector produced by the rotors expressed in the body frame, and  $\mathbf{e}_3 = [0 \ 0 \ 1]^\top$ . Motor throttles  $\boldsymbol{\delta} \in \mathbb{R}^4$ ,  $\delta_i \in [0, 1]$  can be mapped to a total thrust and moment vector using the linear relationship

$$\begin{bmatrix} T \\ \boldsymbol{\tau}^b \end{bmatrix} = \mathbf{M} \boldsymbol{\delta}, \quad (10)$$

where  $\mathbf{M} \in \mathbb{R}^{4 \times 4}$  is an invertible constant mixing matrix that captures vehicle-specific configuration details, such as the position of each rotor with respect to the center of mass, the amount of thrust and torque a single rotor is able to produce, etc. See [13] for more details.

## IV. CONTROLLER ARCHITECTURE

The architecture of the proposed controller is shown in Figure 2. We aim to follow three-times-differentiable trajectories, along with a desired heading and heading rate. The trajectory generator block provides the desired trajectory parameters at time  $t$ , represented by the tuple

$\Gamma(t) = (\mathbf{p}_d(t), \dot{\mathbf{p}}_d(t), \ddot{\mathbf{p}}_d(t), \dddot{\mathbf{p}}_d(t), \psi_d(t), \dot{\psi}_d(t))$ , where  $\mathbf{p}_d(t), \dot{\mathbf{p}}_d(t), \ddot{\mathbf{p}}_d(t), \dddot{\mathbf{p}}_d(t) \in \mathbb{R}^3$  are respectively the desired position, velocity, acceleration and jerk of the body frame with respect to the inertial frame expressed in the inertial frame, and  $\psi_d(t), \dot{\psi}_d(t) \in \mathbb{R}$  are the desired heading and heading rate. A trajectory following LQR controller uses the desired trajectory and the current state to produce a desired force vector  $\mathbf{f} \in \mathbb{R}^3$ . Using the fact that quadrotors are only capable of producing force along the body  $k$ -axis, a desired rotation matrix  $\mathbf{R}_d^i \in \text{SO}(3)$  and angular rate  $\boldsymbol{\omega}_{d/i}^d$  are computed so that the desired  $k$ -axis aligns with the desired force  $\mathbf{f}$ . A geometric controller on  $\text{SO}(3)$  uses these desired rotation states in addition to the current vehicle state to compute the torque the rotors must produce in order to drive the rotational error to zero. The required forces and torques are then mixed using the inverse of (10) to find the required motor throttles, which are then saturated between 0 and 1 before they are fed to the motors on the quadrotor.

## V. TRAJECTORY-FOLLOWING LQR CONTROL

We begin by assuming that the quadrotor is able to produce any desired force  $\mathbf{f}$ , and thus is fully-actuated on  $\mathbb{R}^3$  (we will relax this assumption in the next section). The position and velocity dynamics then become

$$\dot{\mathbf{p}}_{b/i}^i = \mathbf{v}_{b/i}^i, \quad (11a)$$

$$\dot{\mathbf{v}}_{b/i}^i = g\mathbf{e}_3 + \frac{1}{m}\mathbf{f}. \quad (11b)$$

Comparing the current position and velocity with the desired trajectory, we get the error states

$$\mathbf{e}_p = \mathbf{p}_{b/i}^i - \mathbf{p}_d, \quad (12a)$$

$$\mathbf{e}_v = \mathbf{v}_{b/i}^i - \dot{\mathbf{p}}_d. \quad (12b)$$

Taking the time derivative, we get the error dynamics

$$\dot{\mathbf{e}}_p = \mathbf{e}_v, \quad (13a)$$

$$\dot{\mathbf{e}}_v = g\mathbf{e}_3 + \frac{1}{m}\mathbf{f} - \ddot{\mathbf{p}}_d. \quad (13b)$$

Note that these dynamics are linear. Define  $\tilde{\mathbf{f}} = \mathbf{f} - \mathbf{f}_{\text{eq}}$ , where

$$\mathbf{f}_{\text{eq}} = m(-g\mathbf{e}_3 + \ddot{\mathbf{p}}_d) \quad (14)$$

is the force at equilibrium. Then the error state dynamics (13) are represented in state-space form as

$$\dot{\mathbf{e}} = \begin{bmatrix} \mathbf{0} & \mathbf{I} \\ \mathbf{0} & \mathbf{0} \end{bmatrix} \mathbf{e} + \begin{bmatrix} \mathbf{0} \\ \frac{1}{m}\mathbf{I} \end{bmatrix} \tilde{\mathbf{f}}, \quad (15)$$

where  $\mathbf{e} = [\mathbf{e}_p^\top \ \mathbf{e}_v^\top]^\top$ . Additionally, we can augment these error dynamics with the integrator

$$\mathbf{e}_i = \int_0^t \mathbf{e}_p \, dt \quad (16)$$

such that

$$\dot{\mathbf{e}}_a = \underbrace{\begin{bmatrix} \mathbf{0} & \mathbf{I} & \mathbf{0} \\ \mathbf{0} & \mathbf{0} & \mathbf{0} \\ \mathbf{I} & \mathbf{0} & \mathbf{0} \end{bmatrix}}_{\mathbf{A}_a} \mathbf{e}_a + \underbrace{\begin{bmatrix} \mathbf{0} \\ \frac{1}{m}\mathbf{I} \\ \mathbf{0} \end{bmatrix}}_{\mathbf{B}_a} \tilde{\mathbf{f}}, \quad (17)$$

where  $\mathbf{e}_a = [\mathbf{e}_p^\top \ \mathbf{e}_v^\top \ \mathbf{e}_i^\top]^\top$ . These dynamics can easily be shown to be controllable.

Choosing the LQR objective function

$$\mathcal{J}_{\text{LQR}}(\mathbf{e}_a, \tilde{\mathbf{f}}) = \int_0^\infty (\mathbf{e}_a(t)^\top \mathbf{W}_e \mathbf{e}_a(t) + \tilde{\mathbf{f}}(t)^\top \mathbf{W}_f \tilde{\mathbf{f}}(t)) \, dt, \quad (18)$$

where  $\mathbf{W}_e \in \mathbb{R}^{9 \times 9}$  and  $\mathbf{W}_f \in \mathbb{R}^{3 \times 3}$  are symmetric positive definite weighting matrices, the controller that minimizes (18) and exponentially stabilizes the error dynamics (17) is given by

$$\tilde{\mathbf{f}} = -\mathbf{K}\mathbf{e}_a \implies \mathbf{f} = -\mathbf{K}\mathbf{e}_a + \mathbf{f}_{\text{eq}}, \quad (19)$$

where  $\mathbf{K} = \mathbf{R}_f^{-1} \mathbf{B}_a^\top \mathbf{P}_{\text{LQR}}$  and  $\mathbf{P}_{\text{LQR}}$  is the solution to the continuous-time algebraic Riccati equation.

## VI. DESIRED ROTATION

From the trajectory-following LQR controller we receive a desired force vector  $\mathbf{f}$ . In the previous section we assumed that the quadrotor could produce any desired force, but in reality it can only produce force in the direction of its rotors, along the body  $k$ -axis. The vehicle will be able to achieve the desired force only if this axis is aligned with the force vector.

We follow the method presented in [3] to construct a desired rotation matrix  $\mathbf{R}_d^i \in \text{SO}(3)$  (the rotation from the ‘‘desired’’ frame to the inertial frame) such that the desired  $k$ -axis is aligned with  $\mathbf{f}$ . Noting that the columns of a rotation matrix are the coordinate-frame axis vectors, we set  $\mathbf{R}_d^i = [\mathbf{i}_d \ \mathbf{j}_d \ \mathbf{k}_d]$ , where  $\mathbf{i}_d, \mathbf{j}_d$ , and  $\mathbf{k}_d$  are the desired  $i, j$ , and  $k$  coordinate axes expressed in the inertial frame. We set

$$\mathbf{k}_d = -\frac{\mathbf{f}}{\|\mathbf{f}\|} \quad (20a)$$

to align the rotors to the desired force vector. The desired rotation about  $\mathbf{k}_d$  can be chosen arbitrarily. To constrain the rotation matrix, we provide a desired heading  $\psi_d$  from the trajectory generator, implying that

$$\mathbf{j}_d = \frac{\mathbf{k}_d \times \mathbf{s}_d}{\|\mathbf{k}_d \times \mathbf{s}_d\|}, \quad (20b)$$

where  $\mathbf{s}_d = [\cos(\psi_d) \ \sin(\psi_d) \ 0]^\top$ , and

$$\mathbf{i}_d = \mathbf{j}_d \times \mathbf{k}_d. \quad (20c)$$

The desired angular velocity  $\boldsymbol{\omega}_{d/i}^d$  is constructed from the rotational kinematics,

$$\dot{\mathbf{R}}_d^i = \mathbf{R}_d^i \boldsymbol{\omega}_{d/i}^d \implies \boldsymbol{\omega}_{d/i}^d = \left( \mathbf{R}_d^{i\top} \dot{\mathbf{R}}_d^i \right)^\vee, \quad (21)$$

where  $\dot{\mathbf{R}}_d^i = [\dot{\mathbf{i}}_d \ \dot{\mathbf{j}}_d \ \dot{\mathbf{k}}_d]$ , and  $\dot{\mathbf{i}}_d, \dot{\mathbf{j}}_d$ , and  $\dot{\mathbf{k}}_d$  are found by analytically differentiating (20).

Contrary to what is done in [3], we set the total thrust of the motors to be

$$T = \|\mathbf{f}\| \quad (22)$$

as opposed to  $T = -\mathbf{f}^\top \mathbf{R}_b^i \mathbf{e}_3$ . While the latter can be proven to stabilize the full rigid-body dynamics when the

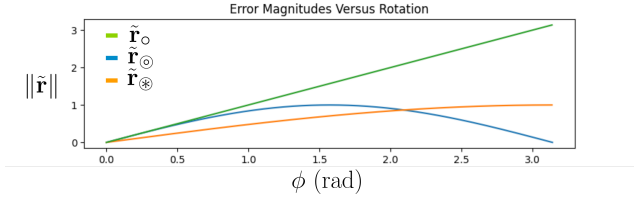


Fig. 3. Error function comparisons.

attitude tracking error is within a bounded region, we found that the former was able to track much more aggressive trajectories.

## VII. CONTROL ON SO(3) USING LOGARITHMIC ERROR

We develop a geometric controller on SO(3) to track the desired rotation  $\mathbf{R}_d^i$  and angular velocity  $\omega_{d/i}^d$  given the rotational dynamics (9c, 9d) and prove that it is globally attractive.

The rotation from the desired frame to the body frame is  $\mathbf{R}_d^b = \mathbf{R}_b^i \mathbf{R}_d^i$ . We evaluate three choices for the error rotation:  $\tilde{\mathbf{r}}_\circ = \frac{1}{2}(\mathbf{R}_d^b - \mathbf{R}_d^{b\top})^\vee$  which comes from using the Lyapunov function  $\frac{1}{2}\text{tr}(\mathbf{I} - \mathbf{R}_d^b)$  [3],  $\tilde{\mathbf{r}}_\circledast = \frac{1}{2\sqrt{1+\text{tr}(\mathbf{R}_d^b)}}(\mathbf{R}_d^b - \mathbf{R}_d^{b\top})^\vee$  used in [6], and the logarithmic map  $\tilde{\mathbf{r}}_\circ = \text{Log}(\mathbf{R}_d^b)$ . Figure 3 shows the magnitude of each error expression versus  $\phi \in [0, \pi]$  given that  $\mathbf{R}_d^b = \text{Exp}([\phi \ 0 \ 0]^\top)$ , where the values of the logarithmic map at  $\phi = 0, \pi$  are determined using the method described in the Appendix. Unsurprisingly,  $\tilde{\mathbf{r}}_\circ$  is the most effective and natural method for representing rotational error since the error increases linearly in  $\phi$ , as would be expected by inverting the geodesic on  $SO(3)$ . For this reason, we choose the rotational error expression to be

$$\tilde{\mathbf{r}} = \tilde{\mathbf{r}}_\circ = \text{Log}(\mathbf{R}_d^b). \quad (23)$$

We express the error in angular velocity as

$$\tilde{\omega} = \mathbf{R}_d^b \omega_{d/i}^d - \omega_{b/i}^b = \omega_{d/b}^b. \quad (24)$$

*Lemma 1:* The dynamics of  $\tilde{\mathbf{r}}$  are given by

$$\dot{\tilde{\mathbf{r}}} = J_l(\tilde{\mathbf{r}})^{-1} \tilde{\omega}, \quad (25)$$

where  $J_l(\tilde{\mathbf{r}})$  is the left Jacobian of SO(3).

*Proof:* We follow the proof given in [7]. Noting that  $\mathbf{R}_d^b = \text{Exp}(\tilde{\mathbf{r}})$ , we take the time derivative to obtain

$$\dot{\mathbf{R}}_d^b = \frac{d}{dt} \text{exp}(\tilde{\mathbf{r}}^\wedge) = \int_0^1 \text{exp}(\alpha \tilde{\mathbf{r}}^\wedge) \dot{\tilde{\mathbf{r}}}^\wedge \text{exp}((1-\alpha)\tilde{\mathbf{r}}^\wedge) d\alpha, \quad (26)$$

where we have used the expression for the time derivative of the matrix exponential. Rearranging, we get

$$\begin{aligned} \dot{\mathbf{R}}_d^b &= \int_0^1 \mathbf{R}_d^{b\alpha} \dot{\tilde{\mathbf{r}}}^\wedge \mathbf{R}_d^{b1-\alpha} d\alpha = \left( \int_0^1 \mathbf{R}_d^{b\alpha} \dot{\tilde{\mathbf{r}}}^\wedge \mathbf{R}_d^{b-\alpha} d\alpha \right) \mathbf{R}_d^b \\ &\implies \dot{\mathbf{R}}_d^b \mathbf{R}_d^{b\top} = \int_0^1 \left( \mathbf{R}_d^{b\alpha} \dot{\tilde{\mathbf{r}}}^\wedge \right)^\wedge d\alpha = \left( \int_0^1 \mathbf{R}_d^{b\alpha} d\alpha \dot{\tilde{\mathbf{r}}}^\wedge \right)^\wedge \\ &= \left( J_l(\tilde{\mathbf{r}}) \dot{\tilde{\mathbf{r}}} \right)^\wedge. \end{aligned} \quad (27)$$

Finally, noting that

$$\dot{\mathbf{R}}_d^b = \mathbf{R}_d^b \omega_{d/b}^d \wedge = \tilde{\omega} \wedge \mathbf{R}_d^b \implies \tilde{\omega} = \left( \dot{\mathbf{R}}_d^b \mathbf{R}_d^{b\top} \right)^\vee, \quad (28)$$

we get

$$J_l(\tilde{\mathbf{r}}) \dot{\tilde{\mathbf{r}}} = \tilde{\omega} \implies \dot{\tilde{\mathbf{r}}} = J_l(\tilde{\mathbf{r}})^{-1} \tilde{\omega}. \quad (29)$$

■

Additionally, the angular velocity error dynamics are given by

$$\mathbf{J} \dot{\tilde{\omega}} = \mathbf{J} \dot{\omega}_{d/i}^b + \omega_{b/i}^b \wedge \mathbf{J} \omega_{b/i}^b - \tau^b, \quad (30)$$

where we note that

$$\begin{aligned} \dot{\omega}_{d/i}^b &= \frac{d}{dt} \left( \mathbf{R}_d^b \omega_{d/i}^d \right) = \mathbf{R}_d^b \dot{\omega}_{d/i}^d + \dot{\mathbf{R}}_d^b \omega_{d/i}^d \\ &= \mathbf{R}_d^b \dot{\omega}_{d/i}^d + \tilde{\omega} \wedge \mathbf{R}_d^b \omega_{d/i}^d \\ &= \mathbf{R}_d^b \dot{\omega}_{d/i}^d - \omega_{b/i}^b \wedge \mathbf{R}_d^b \omega_{d/i}^d. \end{aligned} \quad (31)$$

*Theorem 1:* Given the dynamics (25), and (30), the control law

$$\tau^b = \omega_{b/i}^b \wedge \mathbf{J} \omega_{b/i}^b + \mathbf{J} \dot{\omega}_{d/i}^b + J_l(\tilde{\mathbf{r}})^{-\top} \mathbf{K}_r \tilde{\mathbf{r}} + \mathbf{K}_\omega \tilde{\omega}, \quad (32)$$

where  $\mathbf{K}_r, \mathbf{K}_\omega \in \mathbb{R}^{3 \times 3}$  are symmetric positive definite matrices, will asymptotically drive the error terms  $\tilde{\mathbf{r}}$  and  $\tilde{\omega}$  to zero for all initial values  $\tilde{\mathbf{r}} \neq \pi \mathbf{u}$  and  $\tilde{\omega} \in \mathbb{R}^3$ . Furthermore, if  $\mathbf{K}_\omega = \mathbf{J}$ , then this control law will be globally attractive, even for  $\tilde{\mathbf{r}} = \pi \mathbf{u}$ .

*Proof:* We will first assume that  $\tilde{\mathbf{r}}$  is initially in the set

$$S_1 \triangleq \{\phi \mathbf{u} \mid \phi \neq \pi, \mathbf{u}^\top \mathbf{u} = 1\}. \quad (33)$$

Choose the positive definite Lyapunov function

$$\mathcal{V}(\tilde{\mathbf{r}}, \tilde{\omega}) = \frac{1}{2} \tilde{\mathbf{r}}^\top \mathbf{K}_r \tilde{\mathbf{r}} + \frac{1}{2} \tilde{\omega}^\top \mathbf{J} \tilde{\omega}. \quad (34)$$

Taking the time derivative, we get

$$\begin{aligned} \dot{\mathcal{V}} &= \dot{\tilde{\mathbf{r}}}^\top \mathbf{K}_r \tilde{\mathbf{r}} + \tilde{\omega}^\top \mathbf{J} \dot{\tilde{\omega}} \\ &= \tilde{\omega}^\top J_l(\tilde{\mathbf{r}})^{-\top} \mathbf{K}_r \tilde{\mathbf{r}} + \tilde{\omega}^\top \left( \mathbf{J} \dot{\omega}_{d/i}^b + \omega_{b/i}^b \wedge \mathbf{J} \omega_{b/i}^b - \tau^b \right) \\ &= \tilde{\omega}^\top \left( J_l(\tilde{\mathbf{r}})^{-\top} \mathbf{K}_r \tilde{\mathbf{r}} + \mathbf{J} \dot{\omega}_{d/i}^b + \omega_{b/i}^b \wedge \mathbf{J} \omega_{b/i}^b - \tau^b \right). \end{aligned} \quad (35)$$

Using (32), we get  $\dot{\mathcal{V}} = -\tilde{\omega}^\top \mathbf{K}_\omega \tilde{\omega}$ , which is negative semi-definite. However, note that

$$\begin{aligned} \dot{\mathcal{V}} = 0 &\implies \tilde{\omega} \equiv 0 \implies \dot{\tilde{\omega}} \equiv 0 \\ &\implies \mathbf{J} \dot{\omega}_{d/i}^b + \omega_{b/i}^b \wedge \mathbf{J} \omega_{b/i}^b - \tau^b \equiv 0 \\ &\implies J_l(\tilde{\mathbf{r}})^{-\top} \mathbf{K}_r \tilde{\mathbf{r}} = 0 \\ &\implies \tilde{\mathbf{r}} = 0, \end{aligned} \quad (36)$$

where the last result is due to the fact that the matrix  $J_l(\tilde{\mathbf{r}})^{-\top} \mathbf{K}_r$  is full-rank. Thus, in the set (33), the largest invariant set of the error dynamics (25, 30) is the origin, so by LaSalle's invariance principle [2] the error dynamics are stabilized to the origin by the control input (32).

Now assume that initially  $\phi = \pi$ , therefore  $\tilde{\mathbf{r}}$  is in the set

$$S_2 \triangleq \{\phi \mathbf{u} \mid \phi = \pi, \mathbf{u}^\top \mathbf{u} = 1\}, \quad (37)$$

where the initial body rotation  $\mathbf{R}_b^i$  is exactly 180 degrees from the desired rotation  $\mathbf{R}_d^i$ . In this set the closed-form expressions for the logarithm map (6) and inverse left Jacobian (8) are not well-defined. However, we can use the method described in the Appendix to determine their values. We seek to prove that the set  $S_2$  is not invariant to the dynamics (25) and (30). We will do this by contradiction. First, we note that in order for  $\mathbf{u}$  to stay a unit vector, we have the condition that  $\mathbf{u}^\top \dot{\mathbf{u}} = 0$ . If  $S_2$  is invariant, then  $\dot{\mathbf{u}} = \frac{1}{\pi} \dot{\tilde{\mathbf{r}}}$ . Plugging in, we get

$$\pi \mathbf{u}^\top \dot{\mathbf{u}} = \mathbf{u}^\top J_l^{-1}(\pi \mathbf{u}) \tilde{\boldsymbol{\omega}} = \mathbf{u}^\top \tilde{\boldsymbol{\omega}} = 0, \quad (38)$$

where we have used (50) and the fact that the cross product of any vector with itself is zero. Taking the time derivative of this relationship we get

$$\mathbf{u}^\top \dot{\tilde{\boldsymbol{\omega}}} = -\dot{\mathbf{u}}^\top \tilde{\boldsymbol{\omega}}. \quad (39)$$

However, we see that

$$\begin{aligned} \dot{\mathbf{u}}^\top \tilde{\boldsymbol{\omega}} &= -\frac{1}{\pi} \tilde{\boldsymbol{\omega}}^\top J_l^{-\top}(\pi \mathbf{u}) \tilde{\boldsymbol{\omega}} \\ &= -\frac{1}{\pi} \tilde{\boldsymbol{\omega}}^\top \left( \mathbf{I} + \frac{\pi}{2} \mathbf{u}^\wedge + \mathbf{u}^\wedge \mathbf{u}^\wedge \right) \tilde{\boldsymbol{\omega}} \\ &= -\frac{1}{\pi} \tilde{\boldsymbol{\omega}}^\top \mathbf{u} \mathbf{u}^\top \tilde{\boldsymbol{\omega}} = 0, \end{aligned} \quad (40)$$

where we have used the identity  $\mathbf{u}^\wedge \mathbf{u}^\wedge = -\mathbf{I} + \mathbf{u} \mathbf{u}^\top$ . Therefore we have the condition  $\mathbf{u}^\top \dot{\tilde{\boldsymbol{\omega}}} = 0$  if  $S_2$  is an invariant set. Plugging the control (32) into the angular rate dynamics, we get

$$\mathbf{u}^\top \dot{\tilde{\boldsymbol{\omega}}} = -\pi \mathbf{u}^\top \mathbf{J}^{-1} J_l^{-\top}(\pi \mathbf{u}) \mathbf{K}_r \mathbf{u} - \mathbf{u}^\top \mathbf{J}^{-1} \mathbf{K}_\omega \tilde{\boldsymbol{\omega}} = 0. \quad (41)$$

If we let  $\mathbf{K}_\omega = \mathbf{J}$ , then we have

$$\mathbf{u}^\top \mathbf{J}^{-1} J_l^{-\top}(\pi \mathbf{u}) \mathbf{K}_r \mathbf{u} = 0. \quad (42)$$

Noting that the matrix  $\mathbf{J}^{-1} J_l^{-\top}(\pi \mathbf{u}) \mathbf{K}_r$  is positive definite, this implies that  $\mathbf{u} = 0$ . However, this is contradictory because  $\mathbf{u}$  must be a unit vector. Therefore, for  $\mathbf{K}_\omega = \mathbf{J}$ , the set  $S_2$  is not invariant to the dynamics (25) and 30. Thus  $\tilde{\mathbf{r}}$  will immediately enter the set  $S_1$  and the control (32) is globally attractive. ■

This control law is similar to the one presented in [12] which was shown to be almost-globally exponential stable. However, they neglect the case when  $\phi = \pi$ . To our knowledge, this is the first proof of global attractiveness of a geometric controller on  $\text{SO}(3)$ .

## VIII. SIMULATION EXPERIMENTS

We simulated the quadrotor dynamics (9) and tested the ability of the proposed control scheme to track highly aggressive trajectories. The dynamic parameters we used were  $m = 1$  kg,  $g = 9.81 \frac{\text{m}}{\text{s}^2}$ , and  $\mathbf{J} = \text{diag}(0.07, 0.07, 0.12)$  kg m<sup>2</sup>. To create the mixing matrix  $\mathbf{M}$ , we gave the quadrotor an arm length of 0.25 m, a maximum thrust per rotor of 9.81 N, and a maximum torque per rotor of 5 Nm. Additionally, to demonstrate the robustness of the proposed control scheme we added zero-mean Gaussian input noise to each motor throttle input with a standard deviation of 0.04,

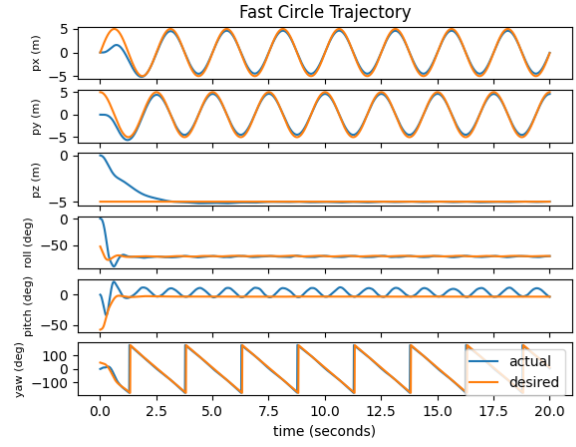


Fig. 4. Fast circle trajectory performance.

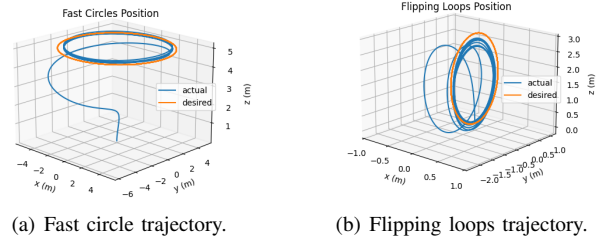


Fig. 5. 3D position plots of the simulated trajectories. The  $z$ -axis of both plots is flipped for visual clarity.

and we perturbed the mixing matrix used in the controller by increasing the estimated thrust per rotor by 10 percent beyond its true value. The control parameters we used were  $\mathbf{W}_e = \text{diag}(2.0, 2.0, 2.0, 1.0, 1.0, 1.0, 10^{-3}, 10^{-3}, 0.1)$ ,  $\mathbf{W}_f = \text{diag}(0.1, 0.1, 1.0)$ ,  $\mathbf{K}_r = \text{diag}(10, 10, 10)$ , and  $\mathbf{K}_\omega = \text{diag}(1.2, 1.2, 1.2)$ . We choose  $\mathbf{K}_\omega \neq \mathbf{J}$  because our simulation is subject to noise, thus the case that  $\tilde{\mathbf{r}} \in S_2$  for all time is extremely unlikely.

### A. Fast Circles

We chose sinusoidal trajectories because of their  $C^\infty$  continuity and because they demonstrate the effectiveness of the proposed control scheme well. For the first trajectory, the quadrotor was commanded to follow circles in the  $xy$ -plane with a diameter of 10 m, a period of 2.5 s, a vertical offset of 5 m, and a commanded heading such that the body  $i$ -axis points in the direction of travel.

The results are shown in Figures 4 and 5(a). The quadrotor converges to the correct altitude within 3 seconds and follows the trajectory fairly well. Due to the aggressiveness of the trajectory and because of the decoupling between the position and rotation controllers, it never quite reaches the correct diameter, but stays fairly close to it. Note that the roll angle throughout the trajectory is around 70 degrees, indicating that the trajectory is quite aggressive.

### B. Flipping Loops

The second trajectory is also sinusoidal. The quadrotor was commanded to do vertical loops in the  $yz$ -plane, with a

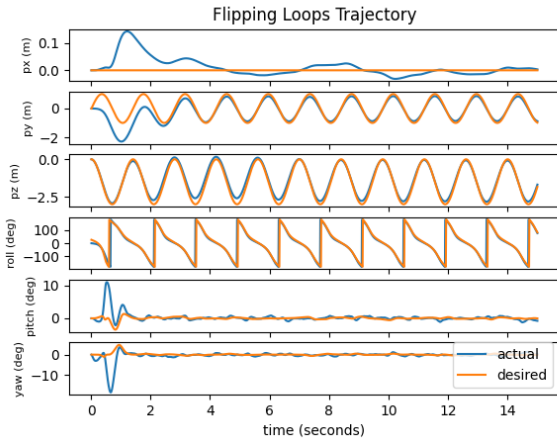


Fig. 6. Flipping loop trajectory performance.

$y$  amplitude of 1 m, a  $z$  amplitude of 1.5 m, a vertical offset of 1.5 m, and a period of 1.4 s. The commanded heading was zero for the entirety of the trajectory. The trajectory is so fast that the only way the quadrotor can follow it is to flip upside-down whenever it reaches the top of the loop in order to accelerate downward faster than gravity.

The results are shown in Figures 6 and 5(b). The quadrotor converges to the trajectory fairly quickly and follows it well. Note that the roll angle continually exceeds 180 degrees, showing that the quadrotor was indeed flipping upside-down.

### C. Upside-down Recovery

For the final trajectory, the quadrotor was given an initial roll angle of exactly 180 degrees and commanded to hover in place at  $\mathbf{p}_d = \mathbf{0}$ . The goal of this trajectory is to verify whether the proposed control scheme is capable of recovering the quadrotor from an upside-down configuration. The performance of our controller was tested against the geometric controller presented in [3]. The results are shown in Figure 7. Our controller only allowed the quadrotor to fall about 6.5 m before it was able to flip the vehicle back over and converge back to the origin. The controller of [3] was unable to recover the quadrotor.

## IX. HARDWARE EXPERIMENTS

### A. Modified Hardware Controller

Most quadrotor hardware platforms have an onboard embedded flight control unit (FCU) that tracks attitude or angular rate commands at very high rates (e.g. 1000 Hz) using an inertial measurement unit (IMU). In order to better interface with the FCU, we modified the controller presented in section VII. We assume that the FCU can achieve a commanded angular rate nearly instantaneously and neglect the angular rate dynamics (9d). Then the rotational dynamics become  $\dot{\mathbf{R}}_b^i = \mathbf{R}_b^i \omega_c^{b\wedge}$ , where  $\omega_c^b$  is the angular velocity command sent to the FCU.

Define  $\tilde{\mathbf{r}}$  and  $\tilde{\omega}$  as in (25, 30), but replace  $\omega_{b/i}^b$  with  $\omega_c^b$ .

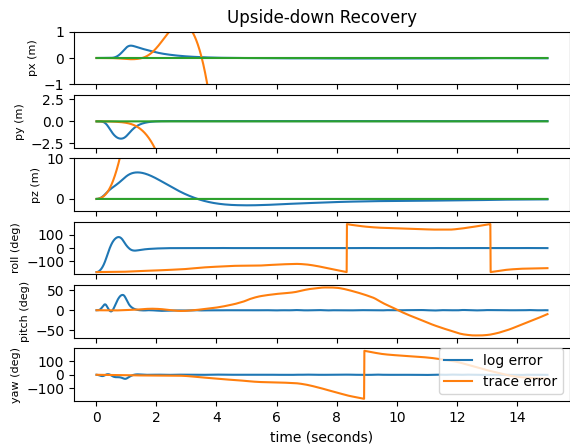


Fig. 7. Upside-down recovery performance, comparing to the controller presented in [3].

*Theorem 2:* The control law

$$\omega_c^b = \mathbf{R}_d^b \omega_{d/i}^d + J_l(\tilde{\mathbf{r}}) \mathbf{K}_r \tilde{\mathbf{r}} \quad (43)$$

exponentially drives the error dynamics (25) to zero for any initial value of  $\tilde{\mathbf{r}}$  (assuming angular velocity is achieved instantaneously).

*Proof:* First, assume that  $\tilde{\mathbf{r}}$  is initially in the set (33). Choose the positive definite Lyapunov function

$$\mathcal{V}(\tilde{\mathbf{r}}) = \frac{1}{2} \tilde{\mathbf{r}}^\top \tilde{\mathbf{r}}. \quad (44)$$

Taking the time derivative, we get

$$\begin{aligned} \dot{\mathcal{V}} &= \dot{\tilde{\mathbf{r}}}^\top \tilde{\mathbf{r}} = \tilde{\omega}^\top J_l(\tilde{\mathbf{r}})^{-\top} \tilde{\mathbf{r}} \\ &= \left( \mathbf{R}_d^b \omega_{d/i}^d - \omega_c^b \right)^\top J_l(\tilde{\mathbf{r}})^{-\top} \tilde{\mathbf{r}}. \end{aligned} \quad (45)$$

Using (43), we get  $\dot{\mathcal{V}} = -\tilde{\mathbf{r}}^\top \mathbf{K}_r^\top \tilde{\mathbf{r}}$ , which is negative definite and can be bounded above by an exponential function of  $\tilde{\mathbf{r}}$ .

We can use a similar argument as the one used in Theorem 1 to show that the set (37) is not invariant to the error dynamics (25). Using (43) and the method for calculating the logarithmic map when  $\phi = \pi$  described in the Appendix, the new error dynamics are

$$\dot{\tilde{\mathbf{r}}} = -\pi \mathbf{u}, \quad (46)$$

which, if the set  $S_2$  is invariant, implies that

$$\dot{\mathbf{u}} = -\mathbf{u}. \quad (47)$$

However, we can immediately see that this is contradictory by multiplying both sides of (47) by  $\mathbf{u}^\top$ , again using the fact that  $\mathbf{u}^\top \dot{\mathbf{u}} = 0$ . Thus the set  $S_2$  is not invariant to the dynamics (25), and the control law (43) is globally attractive. ■

### B. Results

We tested the ability of our control scheme to track aggressive trajectories with a quadrotor hardware platform. Our platform uses ROSFlight<sup>1</sup> as its onboard FCU.

<sup>1</sup>rosflight.org

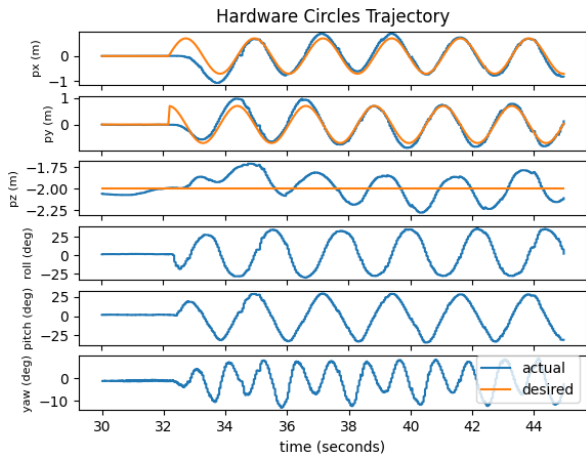


Fig. 8. Hardware circle trajectory performance.

To estimate the state of the quadrotor, we flew the vehicle in a room set up with an Optitrack<sup>2</sup> motion capture system. The control parameters we used were  $\mathbf{W}_e = \text{diag}(0.5, 0.5, 0.5, 0.2, 0.2, 0.2, 0.1, 0.1, 0.1)$ ,  $\mathbf{W}_f = \text{diag}(0.1, 0.1, 0.3)$ , and  $\mathbf{K}_r = \text{diag}(5, 5, 5)$ .

We tested two aggressive trajectories. The first was a 1.4 m diameter circle with a period of 0.45 s, and with a commanded heading of 0. The results are shown in Figure 8. After the trajectory time started at about 32 seconds, the quadrotor quickly converged to the trajectory and was able to track it well throughout the run.

The second trajectory was a hand-designed 5th degree B-spline that started and ended in the same position with no initial or terminal velocity and acceleration. The trajectory was a large loop in the  $yz$ -plane whose required acceleration at the top of the loop is so high that the quadrotor must point its rotors downwards by doing a flip in order to track it. Figure 1 shows a time lapse of the trajectory and Figure 9 shows the results. The quadrotor tracked the  $y$  and  $z$  position fairly well through most of the trajectory, and was completely upside-down just before 30 seconds. After it completed the majority of the maneuver it deviated from the commanded trajectory for a moment. This effect could likely be reduced by further refining the trajectory to ensure dynamic feasibility and/or tuning of the control parameters.

## X. CONCLUSION

We have developed a new quadrotor geometric controller capable of tracking highly aggressive trajectories. Unlike the controller presented in [3], our method uses the logarithmic map to express error in the Euclidean space isomorphic to the Lie algebra of  $\text{SO}(3)$ , which allows us to treat the manifold in a more effective and meaningful manner. Additionally, we have shown the ability of our proposed control scheme to track highly aggressive trajectories in both simulation and hardware experiments.

<sup>2</sup>optitrack.com

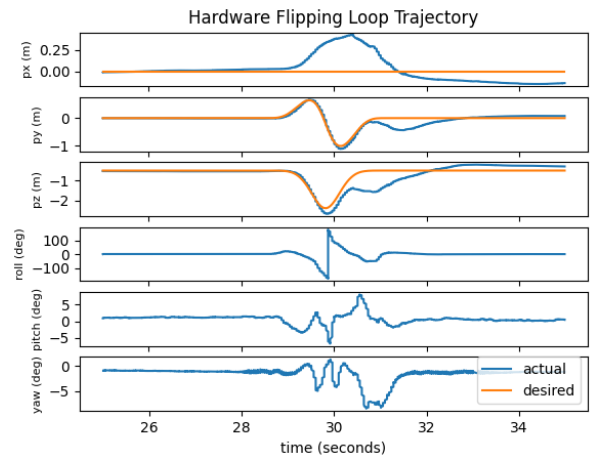


Fig. 9. Hardware flipping loop trajectory performance.

## APPENDIX

### A. The Logarithmic Map at its Singularities

The expression for the logarithmic map (6) is not defined when  $\phi = m\pi$ , where  $m \in \mathbb{Z}$ . For our purposes, we can restrict  $\phi \in (-\pi, \pi]$ . When  $\phi = 0$ , we can use L'Hopital's rule,

$$\text{Log}(\mathbf{R}) = \frac{1}{2}(\mathbf{R} - \mathbf{R}^\top)^\vee = \mathbf{0}, \quad (48)$$

because in this case,  $\mathbf{R} = \mathbf{I}$ . When  $\phi = \pi$ , we can multiply both sides of Equation (4) by  $\mathbf{u}$  to see that

$$\mathbf{u} = \mathbf{R}\mathbf{u}, \quad (49)$$

showing that  $\mathbf{u}$  is an eigenvector of  $\mathbf{R}$  with an eigenvalue of 1. Then we can calculate  $\mathbf{u}$  by performing an eigendecomposition of  $\mathbf{R}$ , and thus have a method for calculating  $\text{Log}(\mathbf{R})$ , even when  $\phi = \pi$ .

In a similar way, we can avoid the singularities of the left Jacobian and its inverse. The expression (7) is not defined at  $\phi = 0$ , and its inverse expression (8) is not defined at  $\phi = 0, \pi$ . In the case where  $\phi = 0$ , we can turn to the infinite series expression of the left Jacobian and its inverse [7] to see that they must both be the zero matrix. In the case where  $\phi = \pi$ , we can use L'Hopital's rule to find that

$$J_l^{-1}(\pi\mathbf{u}) = \mathbf{I} - \frac{\pi}{2}\mathbf{u}^\wedge + \mathbf{u}^\wedge\mathbf{u}^\wedge. \quad (50)$$

## REFERENCES

- [1] S. Bouabdallah, P. Murrieri, and R. Siegwart, "Design and control of an indoor micro quadrotor," in *IEEE International Conference on Robotics and Automation, 2004. Proceedings. ICRA '04. 2004*, vol. 5, 2004, pp. 4393–4398 Vol.5.
- [2] H. K. Khalil, *Nonlinear systems; 3rd ed.* Upper Saddle River, NJ: Prentice-Hall, 2002, the book can be consulted by contacting: PH-AID: Wallet, Lionel. [Online]. Available: <https://cds.cern.ch/record/1173048>
- [3] T. Lee, M. Leok, and N. H. McClamroch, "Geometric tracking control of a quadrotor UAV on  $\text{SE}(3)$ ," in *49th IEEE Conference on Decision and Control (CDC)*, 2010, pp. 5420–5425.
- [4] D. Mellinger and V. Kumar, "Minimum snap trajectory generation and control for quadrotors," in *2011 IEEE International Conference on Robotics and Automation*, 2011, pp. 2520–2525.

- [5] B. Zhou, J. Pan, F. Gao, and S. Shen, "RAPTOR: Robust and perception-aware trajectory replanning for quadrotor fast flight," *IEEE Transactions on Robotics*, pp. 1–18, 2021.
- [6] T. Lee, "Exponential stability of an attitude tracking control system on  $SO(3)$  for large-angle rotational maneuvers," *Systems & Control Letters*, vol. 61, no. 1, pp. 231–237, 2012. [Online]. Available: <https://www.sciencedirect.com/science/article/pii/S0167691111002829>
- [7] T. D. Barfoot, *State estimation for robotics*. Cambridge University Press, 2017.
- [8] J. Solà, J. Deray, and D. Atchuthan, "A micro Lie theory for state estimation in robotics," 2020.
- [9] T. D. Barfoot and P. T. Furgale, "Associating uncertainty with three-dimensional poses for use in estimation problems," *IEEE Transactions on Robotics*, vol. 30, no. 3, pp. 679–693, 2014.
- [10] X.-N. Shi, Y.-A. Zhang, and D. Zhou\*, "Almost-global finite-time trajectory tracking control for quadrotors in the exponential coordinates," *IEEE Transactions on Aerospace and Electronic Systems*, vol. 53, no. 1, pp. 91–100, 2017.
- [11] Y. Yu, S. Yang, M. Wang, C. Li, and Z. Li, "High performance full attitude control of a quadrotor on  $SO(3)$ ," in *2015 IEEE International Conference on Robotics and Automation (ICRA)*, 2015, pp. 1698–1703.
- [12] F. Bullo and R. M. Murray, "Proportional derivative (PD) control on the Euclidean group," 1995.
- [13] R. Mahony, V. Kumar, and P. Corke, "Multirotor aerial vehicles: Modeling, estimation, and control of quadrotor," *IEEE Robotics Automation Magazine*, vol. 19, no. 3, pp. 20–32, 2012.